Peculiarities of magnetoelastic coupling in NiFeGaCo ferromagnetic martensite

S Kustov, M L Corró, E Cesari, J I Pérez-Ladazábal, V Recarte

Peculiarities of magnetoelastic coupling in Ni-Fe-Ga-Co ferromagnetic martensite

S Kustov[1,4], M L Corró[1], E Cesari[1], J I Pérez-Landazábal[2] and V Recarte[2]

[1]Departament de Física, Universitat de les Illes Balears, Cra. Valldemossa, km 7.5, 07122, Palma de Mallorca, Spain

[2]Departamento de Física, Universidad Pública de Navarra, Campus de Arrosadía, 31006 Pamplona, Spain

Sergey.Kustov@uib.cat

The reversible stress-induced magnetization (inverse magnetostriction or Villari effect) has been measured in a polycrystalline Ni-Fe-Ga-Co ferromagnetic martensite. The samples were mechanically excited using longitudinal resonant oscillations at frequencies close to 100 kHz, and experiments were performed over the temperature range 170 – 350 K under variable polarizing fields. It has been found that the reversible inverse magnetostriction changes its sign under low polarizing fields over a certain temperature range with its upper limit close to the Curie temperature. We argue that the variations of sign of the reversible inverse magnetostriction effect are related in the present experiments with the change of the sign of magnetostriction, as has additionally been verified in test measurements performed for pure Ni and Fe. The observed peculiarity of magnetoelastic coupling is also reflected in the temperature dependence of electrical resistance and even produces a minor effect in calorimetry scans. Possible origins of these features of magnetoelastic coupling are discussed.

Keywords: ferromagnet; shape memory alloy; martensite; magnetostriction

PACS: 75.80.+q

Submitted to: Journal of Physics D: Applied Physics

[4] Corresponding author

1. Introduction

Magnetically ordered alloys undergoing a thermoelastic martensitic transformation have been attracting considerable attention due to the possibility of inducing large strains by magnetic field [1,2] and producing high magnetocaloric effect [3,4]. These alloys demonstrate a number of structural modifications, both in the martensitic and parent phases, like magnetic anomalies [5-9] and intermartensitic transformations [10-14] a clear physical origin for which is still lacking. The above mentioned anomalies have been studied by means of measurements of the electrical resistance, calorimetry, elastic and anelastic properties as well as variety of magnetic characteristics.

Recently, a technique for mechanomagnetic spectroscopy has been designed, based on measurements of the reversible inverse magnetostriction effect under periodic stress simultaneously with elastic and anelastic properties of ferromagnetic materials over wide ranges of temperatures, mechanical stress amplitudes and under variable polarizing magnetic field [15]. The designed technique is a new development of previous experimental works in which periodic stress/strain induced magnetization of ferromagnetic materials has been studied [16-19]. In the present work, the following experimental facilities have been introduced in the experimental studies of the reversible inverse magnetostriction: i) determination of the phase of the stress-induced induction (in contrast to just rms values registered before); ii) simultaneous study of magnetic and anelastic properties; and, the most important, iii) possibility to perform the experiments over wide temperature ranges, whereas previously the measurements were made only at ambient temperatures. This technique has already been applied to compare the dynamics of elastic and magnetic domain boundaries in Ni-Fe-Ga polycrystalline ferromagnetic martensites [20]. In the present work we focus our attention on two aspects related to i) methodology of studying magnetoelastic effects, and ii) specific experimental results revealing so far unknown peculiarities of magnetoelastic coupling in ferromagnetic martensites. As far the first aspect is concerned, it should be reminded that the differential direct and inverse magnetostriction effects are linked [21] through the Maxwell relations:

$$\frac{1}{l}\left(\frac{\partial l}{\partial H}\right)_{\sigma} = \left(\frac{\partial B}{\partial \sigma}\right)_{H}, \qquad (1)$$

where *l*, *H*, *B* and σ are the length of the sample, magnetic field, induction and stress, respectively. Applying a method similar to the one used in determining the magnetocaloric effect, one easily obtains from (1) the magnetostriction $\lambda=\Delta l/l$ upon application of a field H^* as a function of differential inverse magnetostriction:

$$\lambda(H^*) = \int_0^{H^*} \frac{1}{l}\left(\frac{\partial l}{\partial H}\right)_\sigma dH = \int_0^{H^*} \left(\frac{\partial B}{\partial \sigma}\right)_H dH \,. \qquad (2)$$

It should be noted here that the experimental method used in the present work yields a periodic magnetic response of the crystal with induction amplitude B_0 to a periodic mechanical stress with an amplitude σ_0, the action of the latter being equivalent to application of a certain anisotropy field H_σ. Estimations have shown that the magnitude of the stress anisotropy field is of the order of only 10 A/m for characteristic stress amplitudes of around 1 MPa [20]. Therefore, in the presence of a static bias field up to 20 kA/m, the periodic stress produces a small oscillatory anisotropy field superimposed on the biasing field. The stress-induced induction in the studied Ni-Fe-Ga-Co alloy is essentially linear with respect to stress amplitude within the range of σ_0 employed, $B_0 \propto \sigma_0$, very much like in the ternary Ni-Fe-Ga system [20]. Therefore, their ratio, following Bozorth notation [21], $\Lambda = B_0/\sigma_0$, is stress-amplitude independent and in the presence of static biasing field should be treated as reversible inverse magnetostriction $\Lambda=\lim_{\sigma_0\to 0}\frac{B_0}{\sigma_0}$. Maxwell-type relations are also fully applicable to the reversible direct and inverse magnetostriction effects, as has been confirmed experimentally for steel [22] and nickel polycrystals [23], reflecting the relationship between the "motor" and "generator" coefficients of a ferromagnet [24]. Therefore, measured stress-induced magnetization reflects not only the reversible inverse magnetostriction, but also, through the Maxwell-type relation, the reversible direct magnetostriction. Thus, plots of B_0/σ_0 versus *H*, or B_0/σ_0 versus *T* (or simply $B_0(H)$ and $B_0(T)$ if the stress amplitude σ_0 is kept constant) reflect correspondingly the field and temperature dependences of

the reversible magnetostriction of the material, so that one can equally well use both these terms to characterize the observed magnetoelastic effects. Reversible and differential characteristics (direct and inverse magnetostriction, permeability) are equal only under hysteresis-free conditions. In that case

$$\lambda(H^*) = \int_0^{H^*} \left(\frac{B_0}{\sigma_0} \right)_H dH \,. \qquad (3)$$

In the presence of hysteresis the reversible magnetostriction differs notably from the differential one [25] and (3) breaks. Moreover, experiments show that the reversible inverse magnetostriction measured in the ultrasonic frequency range is substantially lower than the static one [16]. Nevertheless, we will use (3) later on to evaluate the magnetostriction from reversible inverse magnetostriction in the case of quenched Ni-Fe-Ga-Co samples which demonstrate a very low value of coercive field. Similar estimations will be done also for reference samples of Fe and Ni in order to check the signs and compare the magnitudes of the magnetostriction obtained in these materials using the present technique.

2. Experimental techniques and material

Ultrasonic resonant oscillations of a four component oscillator (two quartz transducers, intermediate non-magnetic bar produced from low-damping Al-Mg alloy and the sample) were generated by means of the equipment described elsewhere [26]. Each element of the composite oscillator, operating at a frequency of around 100 kHz, was measuring half ultrasonic wave length in the corresponding material. The stress-induced induction produced in the sample by an oscillatory stress/strain in a standing wave was detected by a small pickup coil (with a height of 2 mm) placed around the oscillatory stress anti-node in the middle of the sample. The magnitude (modulus) and the phase of the stress-induced induction were determined using an EG&G 5208 lock-in amplifier with an upper frequency limit of 200 kHz. The reference signal was produced from the AC voltage drop on an active resistance by the current flowing through the gauge quartz, which is proportional to and is in phase with the velocity at the end of the transducer [27] (which has the same value for each element of the composite oscillator due to the continuity property). Measurements of the modulus and the phase of the magnetization were performed

for a fixed value of applied magnetic field as a function of temperature and also for different fixed temperatures under cyclic polarizing field. In these experiments the oscillatory amplitude of the sample was typically kept constant at 1×10^{-5} or 2×10^{-5}. The polarizing field was generated by a solenoid with a length of 400 mm, coaxial with the composite oscillator. The constant value or a periodic ramp of the excitation current was produced by means of a KEPCO BOP 72-6 bipolar power supply in the current control mode. The frequency of the current ramp was 0.002 Hz which enabled us to take 256 measurements of resonant frequency, internal friction and stress-induced magnetization for each cycle of polarizing magnetic field.

DSC tests were performed by means of a Mettler DSC 823 calorimeter under a cooling/heating rate of 10 K/min. The real and imaginary parts of the AC electric impedance of the samples were determined over the temperature range 80-400 K by a standard four probe method using EG&G 5204 lock-in amplifier. A squid magnetometer (QD MPMS XL-7 SQUID) was used in measurements of low-field (3.5 Oe and 20 Hz) magnetic AC susceptibility.

A $Ni_{53.5}$-$Fe_{16.5}$-Ga_{27}-Co_3 alloy was produced by induction melting from 99.99% purity elements in Ar atmosphere. Rectangular samples with dimensions of approximately 17×1.5×1.5 mm were spark cut from the ingot, annealed at 1020 K for 1.2 ks and water quenched (WQ) or slowly cooled (SC) in the air. The Curie and the DSC peak temperature of the direct martensitic transformation for the SC samples were found to be 327 and 360 K. Quenching produces a strong martensite stabilization effect in the present alloy [28]. The major feature of the stabilization effect is a substantial shift to higher temperatures of the first reverse transformation after the thermomechanical treatment, which usually disappears in the second and subsequent reverse transformations. In the present alloy the first reverse transformation is displaced to around 570 K. The direct and reverse transformation temperatures registered after the first reverse transformation (when the stabilization effect is removed) return to their values of around 340 and 350 K, respectively. According to the results previously obtained for the present alloy [28], water quenching and slow cooling produce samples with low and high degrees of the long-range atomic ordering, respectively. Quenching results also in a rather diffuse para-ferromagnetic transition, for which the Curie temperature can be estimated as 277 K. Magnetoelastic properties were studied in three WQ and two SC samples, which showed a good reproducibility of data.

Polycrystalline samples of 99.99% purity iron and nickel, for which magnetostriction data are well documented were used as a reference material. Samples were annealed in an evacuated quartz tube for 7 hrs at 1170 K (Fe) and 3 hrs at 1270 K (Ni) and slowly cooled.

3. Experimental results

3.1. Test samples of Fe and Ni

Figure 1 depicts the data on stress-induced induction obtained at 293 K for a test sample of polycrystalline iron. Figure 1(a) shows the magnitude of the magnetic signal under cyclic polarizing field. Full symbols stand for the initial quarter cycle measured for the demagnetized state of the sample, open symbols demonstrate the hysteresis registered in the second cycle of polarizing field. One sees two well-defined minima of the signal for each half cycle of applied field with different polarity. The registered phase of the induction signal with respect to mechanical stress is represented in figure 1(b) by a cycle A-B-C-D-E-F-G-H-I-J. The instantaneous jumps B-C, E-F and H-I of the phase by 360 degrees reflect the change of the range of the measuring device. In addition to these 360 degrees jumps, six rather rapid variations of the phase by ~180°, enumerated from 1 to 6 in figure 1(b), can be observed for each period of applied field. Figure 1(b) depicts also a continuous curve (after correcting the measured data by eliminating the 360 degrees jumps related to the change of the range of lock-in amplifier between -180 and +180 degrees) in which these six variations of phase are clearly visible. Variations of the phase by 180 degrees reflect the change of the sign of the magnetic response to applied stress and coincide with the minima of the induction magnitude, figure 1(a). Two of the phase shifts by 180°, 1 and 4, occur with a large hysteresis, whereas four others – 2,3 and 5,6 - form two pairs of fairly reversible phase variations. The real part of the induction, calculated from the modulus and the phase signal, is represented in figure 1(c). The imaginary part of the stress-induced induction in iron, as well as in the Ni-Fe-Ga-Co alloy studied, remains quite small with respect to the real one, and will be disregarded in the present paper. Two variations of the sign of magnetic induction occur at the points of the loop corresponding to the coercive field H_c. They correspond to the phase variations, 1 and 4, figure 1(b), which occur with a strong hysteresis. Change of the sign of the inverse magnetostriction in points H_c and

$-H_c$ is an obvious effect, related to a change of the direction of preferential magnetic moments alignment without applied stress. As it is well known [29,30], applied stress σ induces uniaxial anisotropy: if $\lambda\sigma > 0$, where λ is the magnetostriction coefficient, the stress direction is an easy axis and magnetic moments tend to align along the applied stress (along the easy axes closest to the stress direction in anisotropic materials), if $\lambda\sigma < 0$, the stress creates an easy plane perpendicular to the stress axis. Thus, for different directions of the internal field (i.e. preferential domain alignment), the same positive (tensile) stress in the case of positive magnetostriction λ will tend to additionally align magnetic moments along the sample axis in opposite directions and therefore will produce the flux variations of different signs through the pickup coil. The same is true for the compressive stress in the case of negative magnetostriction.

The *λ(H)* dependence obtained for the initial quarter of cycle from the demagnetized state of a sample using (3) is also shown in figure 1(c). The data thus derived demonstrate a maximum at around 13 kA/m and a change of the sign at around 16 kA/m. Such behaviour of the fractional length change with applied field is a "signature" of polycrystalline iron, related to the interplay of contributions of positive λ_{100} and negative λ_{111} magnetostriction constants and corresponds well with the results of classical works [29,30]. The real part of the reversible inverse magnetostriction and calculated fractional length change for a Ni sample are shown in figure 2. In full agreement with available data [29,30] *λ(H)* demonstrates no change of the sign of magnetostriction, which is opposite to the sign obtained for Fe in low fields, the absolute values of the magnetostriction being nearly an order of magnitude higher with respect to Fe. The absolute values of magnetostriction calculated from the reversible inverse magnetostriction are substantially lower than the well established data on static fractional change of the length [29,30]. This discrepancy, as discussed in the Introduction section, should be attributed to the existence of the magnetic hysteresis in both materials and using rather high frequencies of around 100 kHz. However, despite the difference in absolute values of magnetostriction obtained from (3) and static fractional length change, the method used detects perfectly qualitative peculiarities of *λ(H)* dependences in both test materials used (e.g., different signs of magnetostriction in polycrystalline Ni and Fe, substantial difference in their absolute values and the change of the sign of λ(H) in Fe for increasing fields). As a

summary, test experiments with reference Fe and Ni samples successfully detect characteristic features of magnetostriction behaviour in these materials despite the restrictions imposed on application of (3) as discussed above in the Introduction section, and, thus, confirm the applicability of this technique to study qualitative peculiarities of magnetoelastic coupling.

3.2. Ferromagnetic Ni-Fe-Ga-Co alloy

Figure 3 shows the temperature spectra of low-field susceptibility for a WQ and SC samples of the Ni-Fe-Ga-Co alloy. The para-ferromagnetic transition is well defined in SC sample, possessing a high degree of long-range atomic order, with a sharp peak at 318 K, just below the Curie temperature of 327 K, determined from the maximum slope of the permeability versus temperature. Such peak in permeability is often referred to as Hopkinson peak and is observed in a variety of ferromagnetic materials, see e.g. [31,32]. On the contrary, the transition is rather diffuse in a disordered WQ sample. The Hopkinson-type peak cannot be detected and the Curie temperature, determined in the same way as in SC sample, is around 277 K.

Figure 4(a) represents the temperature spectra of the magnitude of stress-induced induction registered under constant polarizing field and oscillatory strain amplitude for several WQ and SC Ni-Fe-Ga-Co samples. According to figure 4(a), certain features of the behaviour of the magnetoelastic coupling close to the para-ferromagnetic transition closely remind the data on low-field susceptibility, figure 3: the transition as detected by the inverse magnetostriction is sharp and is also accompanied by the Hopkinson-type peak at 318 K for SC samples, whereas the para-ferromagnetic transition is diffuse in WQ samples. Above the T_c, the inverse magnetostriction gradually decreases with increasing temperature, much like the permeability does. However, one immediately notices an essential difference between the permeability and inverse magnetostriction spectra, which consists in the presence of several minima in the stress-induced magnetization: the first one being situated just above the Curie temperature, the second one well in the ferromagnetic state of the material at around 210-240 K. Figure 4(b) evidences that each minima of the inverse magnetostriction, as in the case of iron samples, figure 1, corresponds to a change of the phase of the stress-induced induction by approximately 180°. In other words, the reversible inverse/direct magnetostriction in Ni-Fe-Ga-Co alloy changes its sign twice: just

above the Curie temperature and at lower temperatures in the ferromagnetic state.

Figure 4(c) indeed demonstrates that the real part of the stress-induced magnetization, calculated from the modulus and the phase data, crosses the temperature axis twice. In each zero-crossing point, the magnetization of the sample is not affected by the applied periodic stress. The points, wherein the magnetization of a ferromagnet looses its sensitivity to applied stress are known as Villari critical points [29]. In the case of a small periodic excitation and reversible magnetostriction, such points have been referred to as differential reversible Villari critical points [16]. The sign of the stress-induced induction at high and low temperature sides of the temperature spectra is the same as in Fe sample for low values of polarizing field. That means that the reversible direct/inverse magnetostriction is positive at high and low temperatures and is negative in the intermediate temperature range. However, observations of change of the sign of reversible inverse magnetostriction in temperature spectra does not necessarily imply the change of the sign of magnetoelastic coupling: the change of the sign of reversible inverse magnetostriction corresponds just to passing through an extremum in $B(\sigma)$ (or $\lambda(H)$) dependence if it is not monotonous and the position of the extremum is temperature-dependent. Studying the reversible inverse magnetostriction as a function of H allows one to clarify whether or not the static magnetostriction λ also changes its sign. Figure 5 (a) to (d) shows the magnitude of the stress-induced induction registered in a WQ sample at different temperatures under cyclic polarizing field. The results demonstrate a dramatic variation of these magnetic "signatures" in the vicinity of zeros of the inverse magnetostriction. The magnetic field dependences show different types of behaviour, with (for example, for temperatures from T=231 to T= 273 K) or without (T=200, 215 K) several minima/maxima, which change qualitatively upon relatively small variations of temperature. Analysis of the in phase component of magnetization, figure 6 (a) to (d), allows one to clarify different tendencies. Over the temperature range from 200 to 266 K the hysteresis loops are very narrow: the hysteresis is even difficult to distinguish in figure 6 (a) and (b). With increasing temperature the loops turn to rotate clockwise (corresponding thus to lower absolute values of magnetoelastic coupling), and, in addition, a dip appears at low polarizing fields whose minimum position is temperature-dependent and which displace the stress-induced induction into the 2nd and 4th quadrants from the 1st and 3rd ones. The positioning of the hysteresis loops in the 2nd and 4th quadrants means that Λ becomes negative. The minimum value of B_0 in

the 2nd quadrant and the maximum in the 4th one are reached at around 250 K, figure 6(b). At higher temperatures, between 250 and 275 K, figure 6(c), the hysteresis loops displace backwards to their initial positions in the 1st and 3rd quadrants. In that case, however, the position of the minima/maxima along the field axis is essentially unchanged. Interestingly, this transformation of hysteresis loops is accompanied by appearance of a notable hysteresis at low applied fields. Between 273 and 288 K, figure 6(d), the motion of the loops towards the 1st and the 3rd quadrants continues. Finally, somewhat above 275 K the loops return completely to their initial positions in the 1st and the 3rd quadrants. Thus, a reversible change of the sign of the inverse and, hence, direct reversible magnetostriction effect takes place over a certain temperature range, which depends on the magnitude of the polarizing field. For high values of polarizing field, the magnetostriction always remains in the 1st and the 3rd quadrants, i.e., it always remains positive. For the external field of 4.25 kA/m these transitions occur around 240 and 275 K, in full agreement with data of figure 3, although the temperature spectra and hysteresis loops shown in figure 6 correspond to different samples.

The very narrow (in the limit, disappearing) hysteresis in WQ samples implies that the reversible inverse/direct magnetostriction becomes closer to the differential one: $\Lambda = \frac{B_0}{\sigma_0} \approx \left(\frac{\partial B}{\partial \sigma}\right)_H = \left(\frac{\partial \lambda}{\partial H}\right)_\sigma$.

Therefore, integration of $\frac{B_0}{\sigma_0}(H)$ loops according to (3) yields in that case a very reasonable estimation for the qualitative behaviour of the field dependence of the static magnetostriction $\lambda(H)$. The results of such integration are depicted in figure 7. We mention first of all that the magnetostriction is positive (like in iron at room temperature and low fields) at high and low temperatures. For the intermediate temperatures and relatively small values of polarizing field (below approximately 18 kA/m) the magnetoelastic coupling changes its sign. The values of polarizing field for which the $\lambda(H)$ dependences change their sign are the Villari (in that case not differential) critical points, wherein the magnetization looses its sensitivity to stress.

Figure 8 depicts similar $B_0(H)$ hysteretic loops for one of the SC samples. Two plots, figures 8(b) and 8(d), again reflect the behaviour of the alloy close to the two differential Villari critical points. The most striking difference between WQ and SC samples is that the hysteresis is practically absent in the former

below the Curie temperature, figure 6, whereas the hysteresis is quite wide in the latter. However, similar to the WC samples, the hysteresis loops change their positions in the vicinity of the two differential Villari points from the 1st and 3rd quadrants to the 2nd and the 4th and vice versa. Existence of the hysteresis facilitates observation of the fact that simultaneously with such rotation of the loops, the change of the direction of the circulation along the loops takes place. This effect can be illustrated by figure 8(b). One sees that on lowering temperature from 262.4 K to 250 K a "neck" appears in the middle part of the loop, the direction of the circulation being the same. In between 250 and 244 K the two parts of the formed "neck" collapse and switch their positions. This results in the inversion of the circulation direction along the central part of the loop, keeping, however, the former direction of the circulation close to the extremities of the loops. The latter completely disappears upon further cooling by just a few degrees down to 240 K. Figures 8(d) and 6(d) demonstrate that, despite the substantial difference in the coercive force between SC and WQ samples below the Curie temperature, the behaviour of the loops close to the differential Villari point just above T_c is essentially the same. The presence of a significant magnetic hysteresis in SC samples does not allow one to obtain the $\lambda(H)$ dependences similar to those for WQ samples, figure 7. Nevertheless, we believe that the similarity of the temperature spectra (figure 4) and of the effect of temperature and magnetic field on the $B_0(H)$ dependences (figure 8) give a clear evidence of a similar change of the sign of magnetoelastic coupling in SC samples as in the WQ ones.

4. Discussion

4.1. Villari critical line in H-T plane

The present results, as shown in figure 7, indicate that the magnetostriction λ in the Ni-Fe-Ga-Co alloy is negative over certain temperature-polarizing field domain and positive otherwise. Thus, a Villari critical line can be drawn on the *H-T* plane, separating domains with positive and negative magnetostriction, as is shown in figure 9. The high-temperature limit of the region of negative magnetostriction is close to the Curie temperature, just where the magnetic domain structure is being formed. This fact is confirmed by the simultaneous shift of this high-temperature limit together with the T_c for WQ and SC samples, in

which the Curie temperatures are substantially different. In general, one should not be surprised that certain magnetoelastic coupling can be detected above the T_c. For example, the exchange magnetostriction can be detected in Ni at least some 150 K above the T_c [33].

4.2. Width of magnetoelastic hysteresis in quenched and aged samples

A very narrow hysteresis of magnetoelastic coupling registered in quenched samples and a broad one in slowly cooled ones look strange, since quenched samples contain more defects, which are expected to impede the mobility of domain walls. Indeed, the studies of magnetization loops for a $Ni_{50}Mn_{27}Ga_{23}$ alloy reveal an opposite tendency: the coercivity is higher for disordered samples than for ordered ones [34]. In this respect, it is worthwhile to comment, first of all, that the width of domain walls in ferromagnetic materials is rather high. The magnetization vector rotates in a 180° degree Bloch wall over the distance [35] $L \approx 4l_{ex}\sqrt{\frac{\mu_o M_s^2}{2K_1}}$, where l_{ex} is the exchange length, M_s and K_1 are the saturation magnetization and anisotropy constant, respectively. Taking the magnetocrystalline anisotropy constant for a Ni-Fe-Ga-Co alloy of similar composition K_1~ 1×10^5 kJ/m^3 [36] and the characteristic values of the exchange length l_{ex}~30 Å [35], $\mu_0 M_s$~1 T, one obtains L~100 Å. On the other hand, quenched ferromagnetic shape memory alloys possess a low degree of long-range $L2_1$ order and very small ordered domain size, with a characteristic dimension in ternary Ni-Fe-Ga alloys of the order of only 100-300 Å [37]. Ordered samples, on the contrary, possess high degree of atomic order and ordered domains ~ 2000 Å [37]. Antiphase domain boundaries are known as efficient pinners of the magnetic domain walls [34,38]. However, the size of ordered domains in WQ samples is of the same order of magnitude as the width of the magnetic domain wall. That means that, statistically, all positions of a magnetic domain wall with respect to the antiphase boundaries are equivalent, meaning that the pinning effect is absent. On the contrary, in ordered samples the ordered domain size is much higher than the magnetic domain wall width and antiphase boundaries represent efficient obstacles for domain walls. Another interesting observation, related to the abovementioned interpretation is that WQ and SC samples demonstrate similar hysteresis above the Curie temperature, where the magnetic domains are not as yet formed and only short-range magnetic ordering exists. Under these circumstances, i.e. somewhat above the T_c, the

coercive force for WQ samples becomes even much higher than well in the ferromagnetic state, cf. figures 6(c) and 6(a), although the magnitude of magnetoelastic coupling is very low above the T_c as compared to the ferromagnetic state. Opposite effects of the degree of ordering on the magnetic hysteresis obtained in the present work and reported in [34] are probably related to substantially larger antiphase domains in Ni-Mn-Ga than in Ni-Fe-Ga alloys. Indeed, even in WQ Ni-Mn-Ga samples the domain size can be estimated as being of the order of 100 nm [39], whereas in ordered samples the domain size exceeds ~ 10^3 nm. Under these circumstances, antiphase domain boundaries become efficient pinners even in WQ samples. Since WQ samples have higher density of antiphase boundaries (which are now efficient pinners) than ordered samples, the coercivity of disordered samples is higher than that of the ordered ones.

4.3. Other manifestations of the peculiarities in magnetoelastic coupling.

The observed variations of sign of magnetoelastic coupling are limited to the range of rather low applied fields. Therefore, they can be detected by magnetic as well as by any other type of measurements only under low magnetic fields, whereas any possible anomaly should disappear for measurements under high fields. This is exactly the feature of the anomalies observed in the temperature dependence of the magnetic susceptibility in ternary Ni-Fe-Ga martensite over similar temperature range [9]. From this point of view, one can speculate that the observed peculiarities of the magnetoelastic coupling in ferromagnetic martensites can be the driving force for the variety of the abovementioned structural/microstructural rearrangements [5-14] detected by calorimetry, resistivity and internal friction measurements, since these experiments are performed typically under zero applied field. Additional calorimetry and AC impedance measurements have been performed in order to verify this hypothesis.

Figure 10 shows the temperature spectra of the real part of the AC impedance of the SC sample. The data in figure 10 were obtained for a low frequency of 21.7 Hz, making negligible the contribution of skin-effect to the real part of the AC impedance [40]. Therefore, the resistance in figure 10, although measured with AC, asymptotically reflects the direct current resistance. The parts of the temperature spectrum below ~ 230 K and above this temperature up to the T_c can very well be fitted by straight lines, with a change of the slope close to the Villari critical point. Two different samples showed similar

behaviour, reproducible on cooling and heating, much like the observed anomaly of the magnetoelastic coupling. Thus, resistivity data clearly demonstrate a change of the temperature coefficient of the resistance just at the Villari critical point.

Figure 11 shows the results of the calorimetry tests performed for a SC sample. Similar data were obtained for 5 different SC samples. One can distinguish small peculiarities of the heat flow at temperatures of around 320 and 240 K, which correspond to the T_c and the observed Villari critical point. In fact, since the high-temperature Villari critical point is close to the T_c temperature, they cannot be separated in the DSC results. One can notice even a slight change of the slope of the DSC curve both at 240 and 320 K, pointing to a change of the heat capacity value. It is tempting thus, based on the results of DSC and AC impedance studies, to conclude that the observed variations of the sign of magnetoelastic coupling slightly affect also transport and thermodynamic properties of the Ni-Fe-Ga-Co alloy.

4.4. Possible origins of variation of sign of the magnetoelastic coupling

Although the polycrystalline ferromagnets are isotropic through compensation, the isotropic treatment of magnetostriction is not appropriate. For example, for crystals with cubic symmetry the anisotropic saturation magnetostriction of a polycrystalline aggregate without texture, obtained by averaging of strain over each crystallite, is a linear combination of two magnetostriction coefficients, $\lambda^{\gamma,2}$ and $\lambda^{\varepsilon,2}$ [30]. If these coefficients have different signs, the magnetostriction of a polycrystalline aggregate can demonstrate non-monotonous dependence or even a change of sign, for example as a function of applied field [29]. Polycrystalline iron is a classical example of such situation [29,30]. Thus, changes of the sign of magnetoelastic coupling in a temperature domain, observed in the present work, can be attributed to a similar mechanism, assuming that some of the magnetostriction coefficients in low-symmetry martensitic phase have opposite signs and demonstrate different temperature dependence. This hypothesis implies that just a smooth variation with temperature and applied magnetic field of the linear combination of the magnetostriction constants occurs, which produces the change of the sign of net magnetostriction in polycrystalline aggregates. However, according to this scenario, no anomalies are expected in the resistivity and DSC data, which actually point to substantial structural/microstructural

rearrangements occurring at the Villari critical line. Therefore, one cannot discard another interpretation of the observed peculiarity of magnetoelastic coupling, related to possible changes of signs of magnetoelastic constants themselves. Namely, the contributions of two- and single-ion coupling to anisotropic magnetoelastic coupling coefficients can be of the same order of magnitude and have opposite signs, and in that case, the anisotropic magnetostriction coefficients can demonstrate extrema or changes of sign [30].

Unfortunately, low symmetry of martensite and polyvariant structure of samples makes difficult the use of single crystalline samples to distinguish between the two possible mechanisms discussed. However, we believe that observation of sharp minima in temperature spectra of inverse magnetostriction in the austenitic phase of a polycrystalline ternary Ni-Fe-Ga alloy [15] reflects the existence of similar variation of sign of magnetoelastic coupling in the austenitic cubic phase as well. Therefore, investigation of austenitic single crystals of different orientation should provide a key to identify the specific origin of the observed peculiarity of magnetoelastic coupling. This work is ongoing.

5. Conclusions

- Measurement of the inverse magnetostriction effect is an efficient and convenient method of investigations of the magnetoelastic coupling in ferromagnetic materials.

- The inverse and direct magnetostriction in a polycrystalline Ni-Fe-Ga-Co ferromagnetic shape memory alloy demonstrates a variation of its sign over a certain temperature range. The variation of the sign of magnetoelastic coupling is restricted to low values of polarizing field. We suggest that the observed peculiarity of the magnetoelastic coupling might be at the origin of as yet not well understood structural/microstructural effects detected in ferromagnetic shape memory alloys by calorimetry, internal friction, resistivity and also in magnetic properties at low polarizing fields.

Acknowledgement

The authors are grateful to Prof. D.N. Beshers (Columbia University) for fruitful discussions. The work was supported by FEDER and DGI, Spain, through the projects MAT2006-28193-E, MAT2008-01587 and MAT 2009-07928.

References

[1] Ulakko K, Huang J K, Kantner C, O´Handley R C and Kokorin V V 1996 *Appl. Phys. Lett*. **69** 1966.

[2] Murray S J, Marioni M, Allen S M and O'Handley R C 2000 *Appl. Phys. Lett*. **77** 886.

[3] Zhou X, Li W, Kunkel H P and Williams G 2004 *J. Phys.: Condens. Matter* **16** L39.

[4] Krenke T, Duman E, Acet M, Wassermann E F, Moya X, Mañosa Ll and Planes A 2005 *Nat. Mater.* **4** 450.

[5] Pakhomov A B, Wong C Y, Zhang X X, Wen G H and Wu G H 2001 *IEEE Transactions on Magnetics* **37** 2718.

[6] Murakami Y, Shindo D, Oikawa K, Kainuma R and Ishida K 2003 *Appl. Phys. Lett*. **82** 3695.

[7] Majumdar S, Sharma V K, Manekar M, Kaul R, Sokhey K J S, Roy S B and Chaddah P 2005 *Solid State Comm*. **136** 85.

[8] Sharma V K, Chattopadhyay M K, Kumar R, Ganguli T, Kaul R, Majumdar S and Roy S B 2007 *J. Phys. D: Appl. Phys*. **40** 3292.

[9] Pérez-Landazabal J I, Recarte V, Gómez-Polo C, Seguí C, Cesari E and Dutkiewicz J 2008 *Mater. Sci. Engn*. A **481-482** 318.

[10] Khovailo V V, Oikawa K, Wedel C, Takagi T, Abe T and Sugiyama K 2004 *J. Phys.: Condens. Matter* **16** 1951.

[11] Chernenko V A, Cesari E, Khovailo V, Pons J, Seguí C and Takagi T 2005 *J. Magn. Mag. Mater*. **290–291** 871.

[12] Kokorin V V, Perekos A O, Tshcherba A A, Babiy O M and Efimova T V 2006 *J. Magn. Mag. Mater.* **302** 34.

[13] Seguí C, Pons J and Cesari E 2007 *Acta Mater*. **55** 1649.

[14] Hamilton R F, Sehitoglu H, Efstathiou C and Maier H J 2007 *Acta Mater*. **55** 4867.

[15] Kustov S, Masdeu F and Cesari E 2006 *Appl. Phys. Lett*. **89** 061917.

[16] Pravdin L S 1982 *Soviet Journ. Non-Destructive Testing* **18** 613.

[17] Ruuskanen P and Kettunen P 1991 *J. Mag. Magn. Mater*. **98** 349.

[18] Coronel V F, Beshers D N, Catto S and Ryan F S 1994 *J. Phys. Chem. Solids* **55** 1521.

[19] Hatafuku H 2002 *Electrical Engineering in Japan* (Denki Gakkai Ronbunshu) **140** 1.

[20] Kustov S, Corró M and Cesari E 2007 *Appl. Phys. Lett*. **91** 141907.

[21] Bozorth R M 2003 *Ferromagnetism*, ed Willey J (USA: IEEE Press) p. 732.

[22] Pravdin L S, Vlasov K B and Rodigin N M 1980 *Phys. Met. Metall.* **47** 41.

[23] Vlasov K B and Pravdin L S 1981 *Phys. Met. Metall*. **48** 101.

[24] Jiles D C 2003 *Acta Mat*. **51** 5907.

[25] Bozorth R M 2003 *Ferromagnetism*, ed Willey J (USA: IEEE Press) p. 641.

[26] Kustov S, Golyandin S, Ichino A and Gremaud G 2006 *Mater. Sci. Engn*. A **442** 532.

[27] Robinson W H and Edgar A 1974 *IEEE Trans. on Sonics and Ultrasonics* **SU-21** 98.

[28] Picornell C, Pons J, Cesari E and Dutkiewicz J 2008 *Intermetallics* **16** 751.

[29] Bozorth R M 2003 *Ferromagnetism*, ed Willey J (USA: IEEE Press) p. 968.

[30] Du Trémolet de Lacheisserie É, Gignoux D and Schlenker M 2005 *Magnetism. Fundamentals*, (USA: Springer) p. 507.

[31] Salas F and Mirabal-García M 1990 *Phys. Rev. B* **41** 10859.

[32] Blázquez J S, Franco V, Conde C F, Conde A and Kiss L F 2007 *J. Alloys Comp*. **431** 100.

[33] Kollie T G 1977 *Phys. Rev. B* **16** 4872.

[34] Venkateswaran S P, Nuhfer N T and De Graef M 2007 Acta materialia **55** 5419.

[35] Bertotti G 1998 *Hysteresis in Magnetism*, (USA: Academic Press) p. 198.

[36] Morito K, Fujita A, Oikawa K, Ishida K, Fukamichi K and Kainuma R 2007 *Appl. Phys. Lett*. **90** 062505.

[37] Oikawa K, Ohmori T, Tanaka Y, Morito H, Fujita A, Kainuma R, Fukamichi K and Ishida K 2002 *Appl. Phys. Lett*. **81** 5201.

[38] Yu X Z, Asaka T, Tomioka Y, Kaneko Y, Uchida M, He J P, Ngai T, Kimoto K, Matsui Y and Tokura Y 2007 *Journ. Mag. Magn. Materials* **310** 1572.

[39] Venkateswaran S P, Nuhfer N T and De Graef M 2007 *Acta materialia* **55** 2621.

[40] Corró M L, Kustov S and Cesari E 2009 *Journ. Appl. Phys*. **105** 073519.

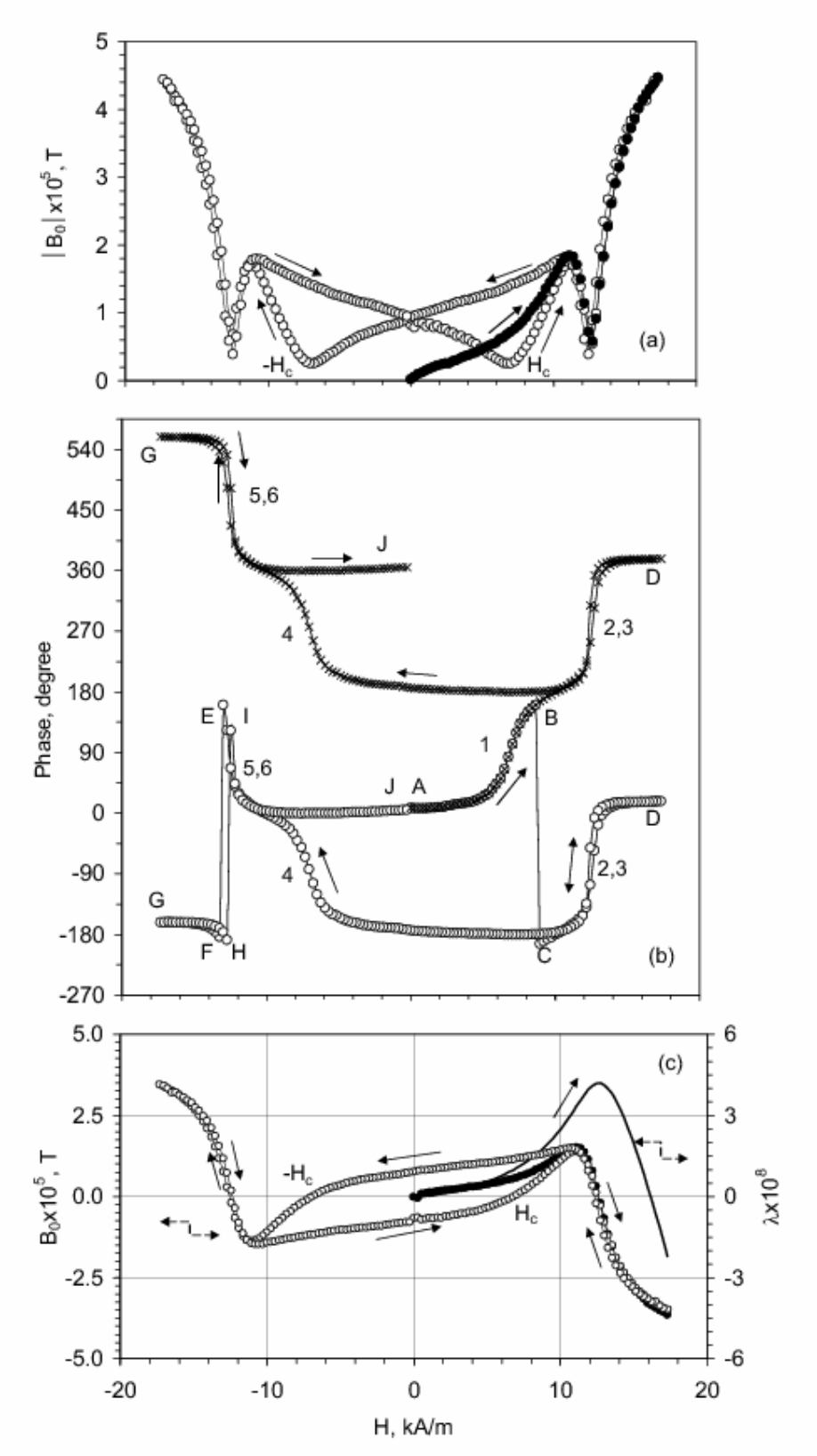

Figure 1. Stress-induced induction of a polycrystalline sample of Fe (ultrasonic strain amplitude of 1×10^{-5}, temperature T=293 K) versus cyclic polarizing field with a frequency of 0.002 Hz: a) absolute value of the

amplitude of stress-induced induction; b) phase of the induction with respect to strain/stress amplitude; letters A to J indicate a full cycle of phase variation, numbers from 1 to 6 – rapid variations of the phase by 180 degrees. Open symbols represent the phase measured in experiment, crosses – values after correction of jumps B-C, E-F, I-H of 360 degrees corresponding to the changes of range of the measuring device between + 180 and -180 degrees; c) real part of the amplitude of the stress-induced induction. Data are shown for the second cycle of applied field, full symbols in (a) and (c) stand for the first quarter of the cycle starting from the demagnetized state of the sample. Solid line in (c) shows the result of the integration, according to (3), of the real part of the B_0/σ_0 ratio for the first quarter cycle of polarizing field starting from the demagnetized state of the sample. Arrows indicate the direction of field change.

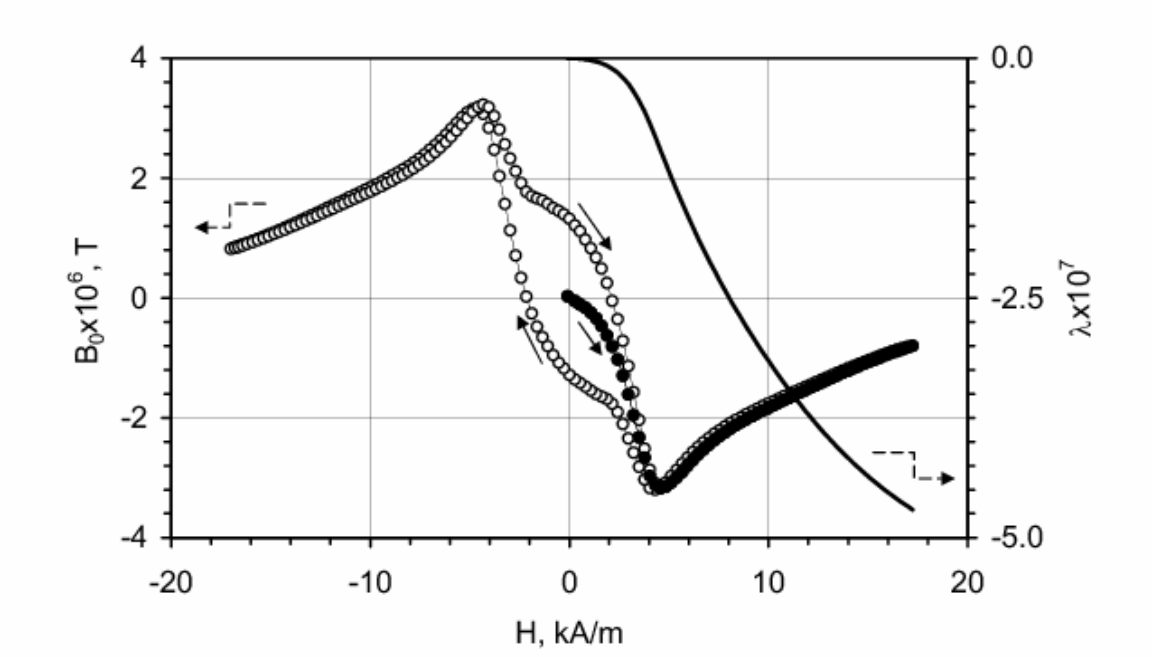

Figure 2. Real part of the amplitude of the stress-induced induction in a polycrystalline Ni sample (ultrasonic strain amplitude 3×10^{-7}, temperature 293 K) versus cyclic polarizing field with a frequency of 0.002 Hz. Empty symbols stand for the second cycle of polarizing field, full symbols – for the first quarter cycle starting from demagnetized state. Solid line shows the result of the integration, according to (3), of the real part of the B_0/σ_0 ratio for the first quarter cycle of polarizing field starting from the demagnetized state of the sample.

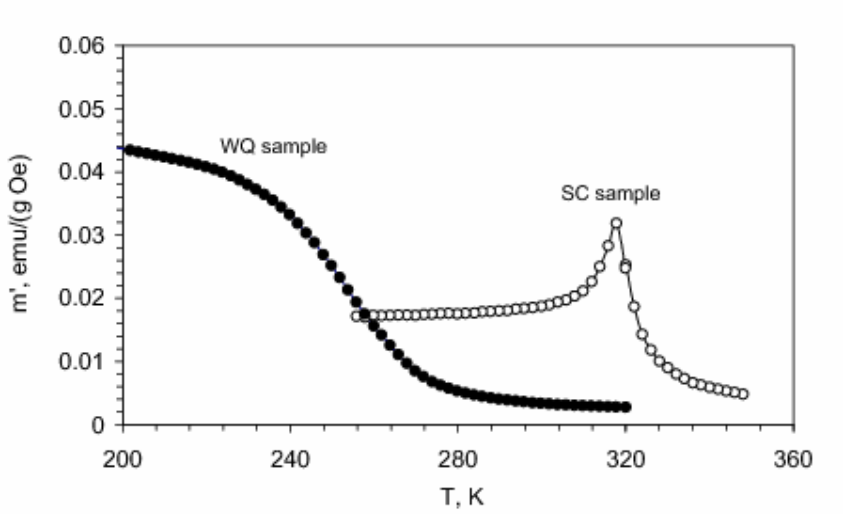

Figure 3. Temperature spectra of the low-field susceptibility for water quenched (WQ) and slowly cooled (SC) samples of a polycrystalline $Ni_{53.5}$-$Fe_{16.5}$-Ga_{27}-Co_3 alloy.

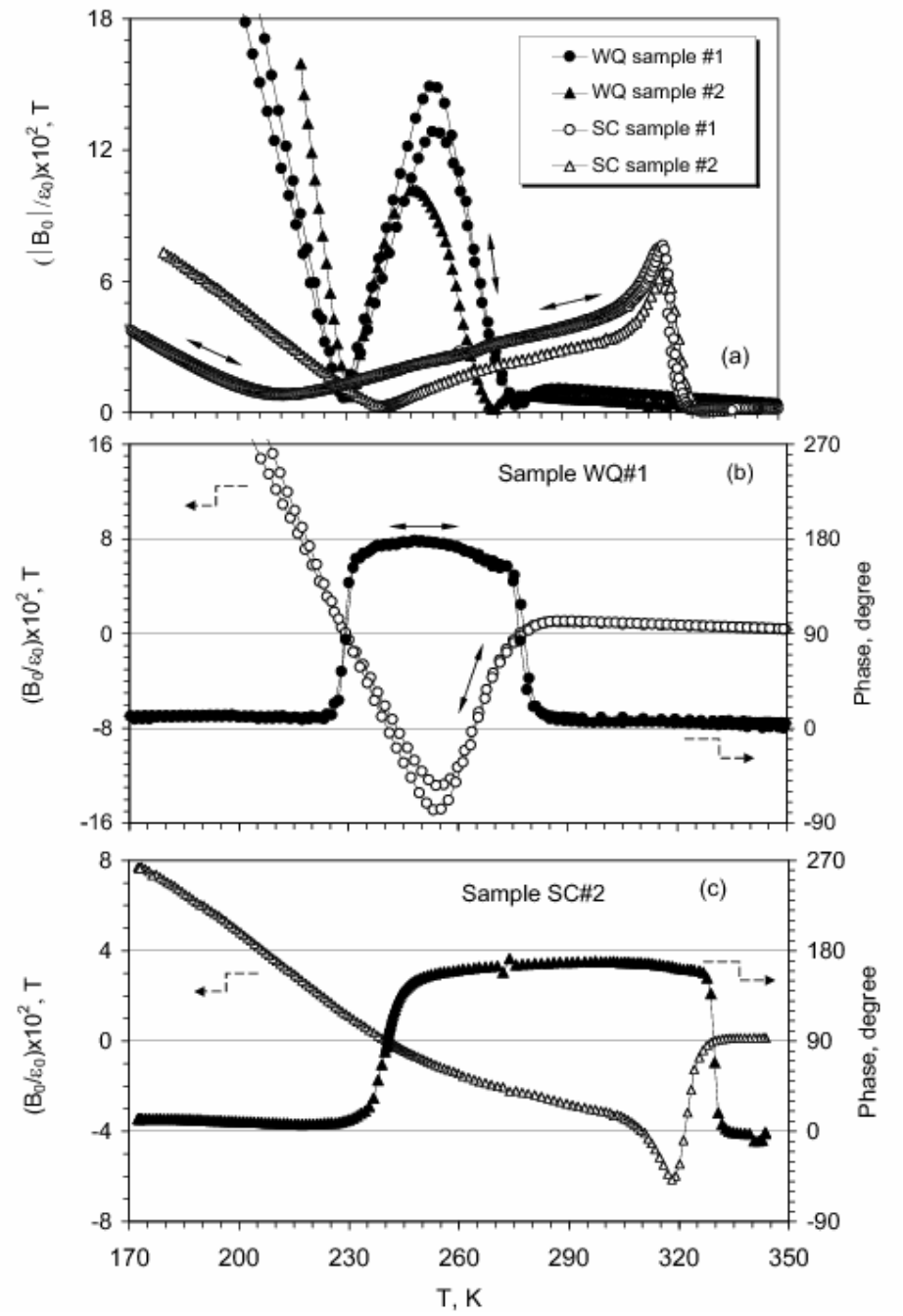

Figure 4. Temperature spectra of stress-induced induction of water quenched (WQ) and slowly cooled (SC) samples of a polycrystalline $Ni_{53.5}$-$Fe_{16.5}$-Ga_{27}-Co_3 alloy under constant values of oscillatory strain amplitude and polarizing field: a) absolute value of the amplitude of stress-induced induction normalized by oscillatory strain amplitude; (b), (c) - phase and the real part of the induction with respect to strain/stress for the water quenched and slowly cooled samples, respectively. WQ sample#1: oscillatory strain amplitude of 2×10^{-5}, polarizing field 4.25 kA/m;WQ sample#2: oscillatory strain amplitude of 1×10^{-5}, polarizing field 2.8 kA/m;SC sample #1: oscillatory strain amplitude of 2×10^{-5}, polarizing field 2.8

kA/m; SC sample #2: oscillatory strain amplitude of 1×10^{-5}, polarizing field 2.8 kA/m. For WQ sample #1 and SC sample#1 data for cooling and heating scans are shown to demonstrate reversibility of the data, WQ sample #2, SC sample #2 –measurements during cooling.

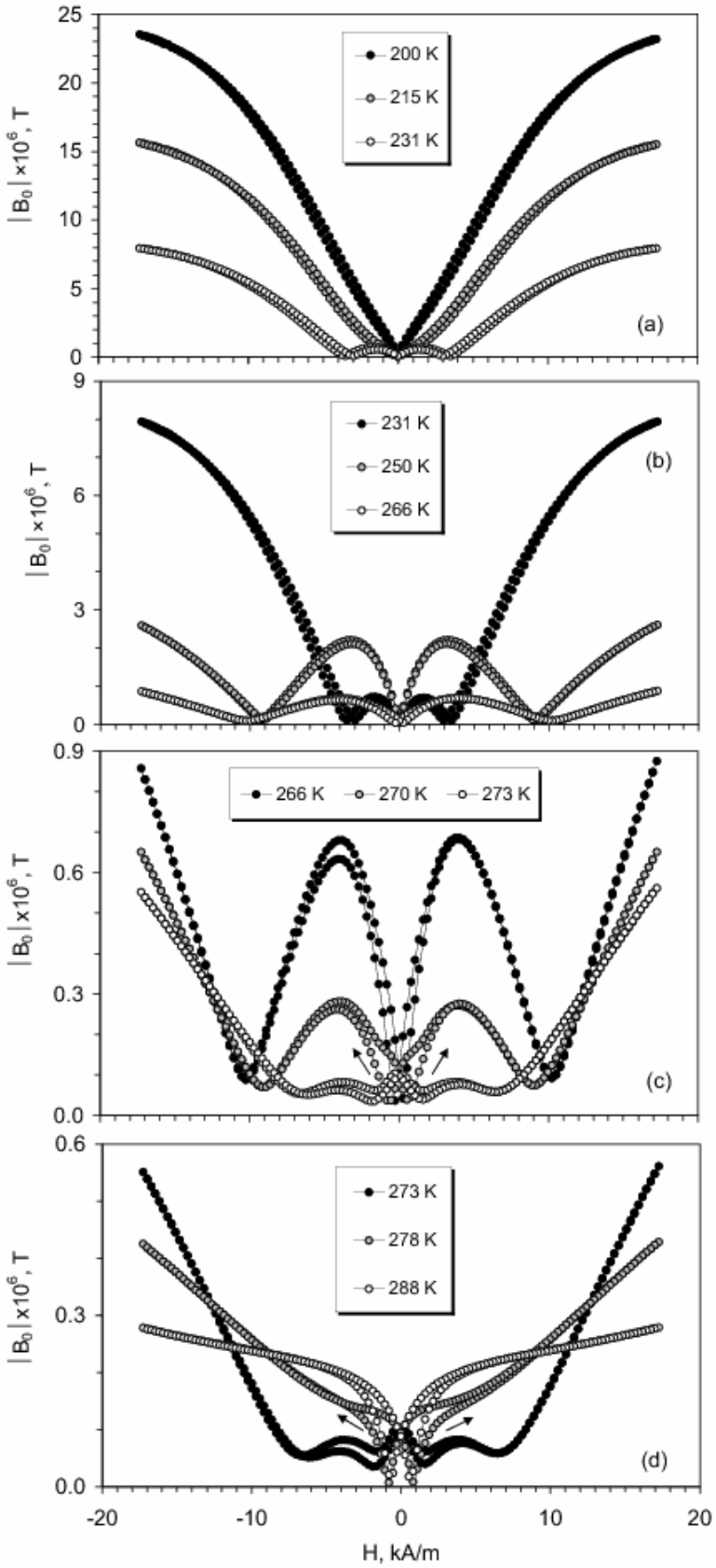

Figure 5. Absolute values of the amplitude of stress-induced induction for a water quenched sample #2 of

a Ni-Fe-Ga-Co alloy (ultrasonic strain amplitude of 2×10^{-5}) versus cyclic polarizing field with a frequency of 0.002 Hz for temperatures 200-231 K (a), 231-266 K (b), 266-273 K (c) and 273-288 K (d). Arrows show directions of the circulation along the loops.

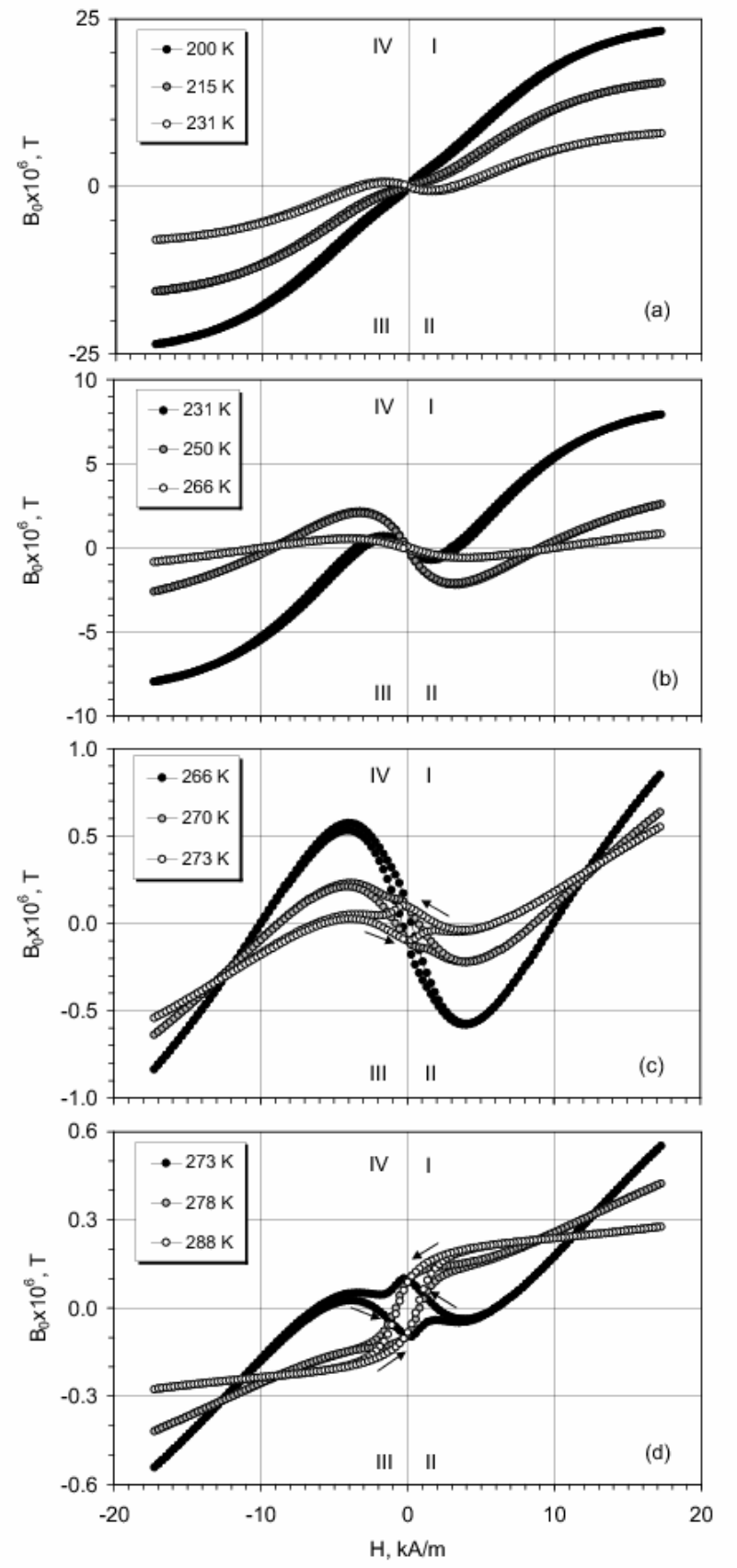

Figure 6. Real part of the stress-induced induction (corresponding to the data in figure 5) versus cyclic

polarizing field. Arrows show directions of circulation along the loops.

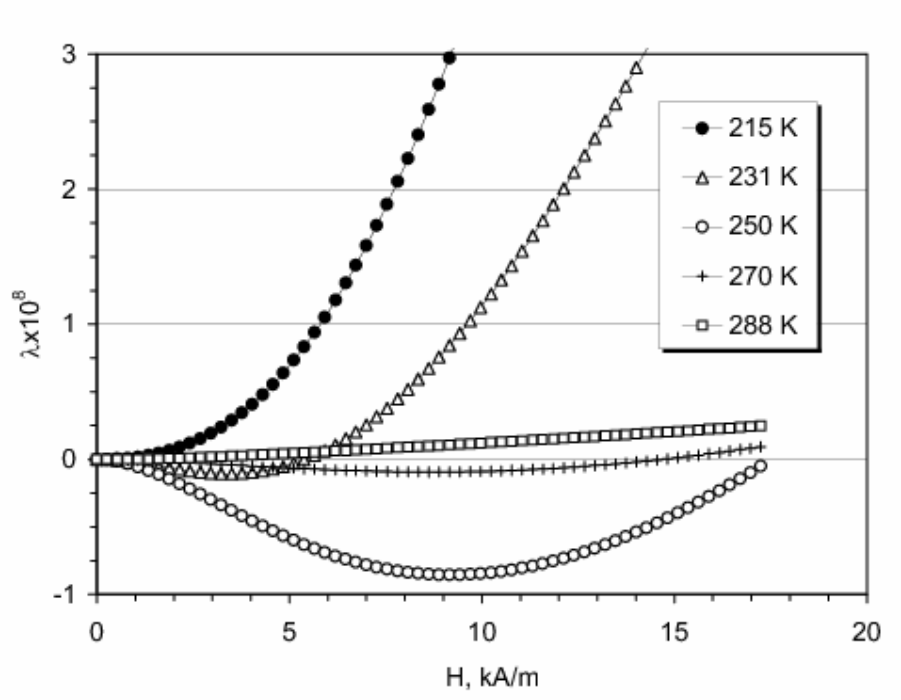

Figure 7. Field dependences of the direct/inverse magnetostriction for several temperatures, as obtained by integration of first quarter cycles of hysteresis loops from figure 6.

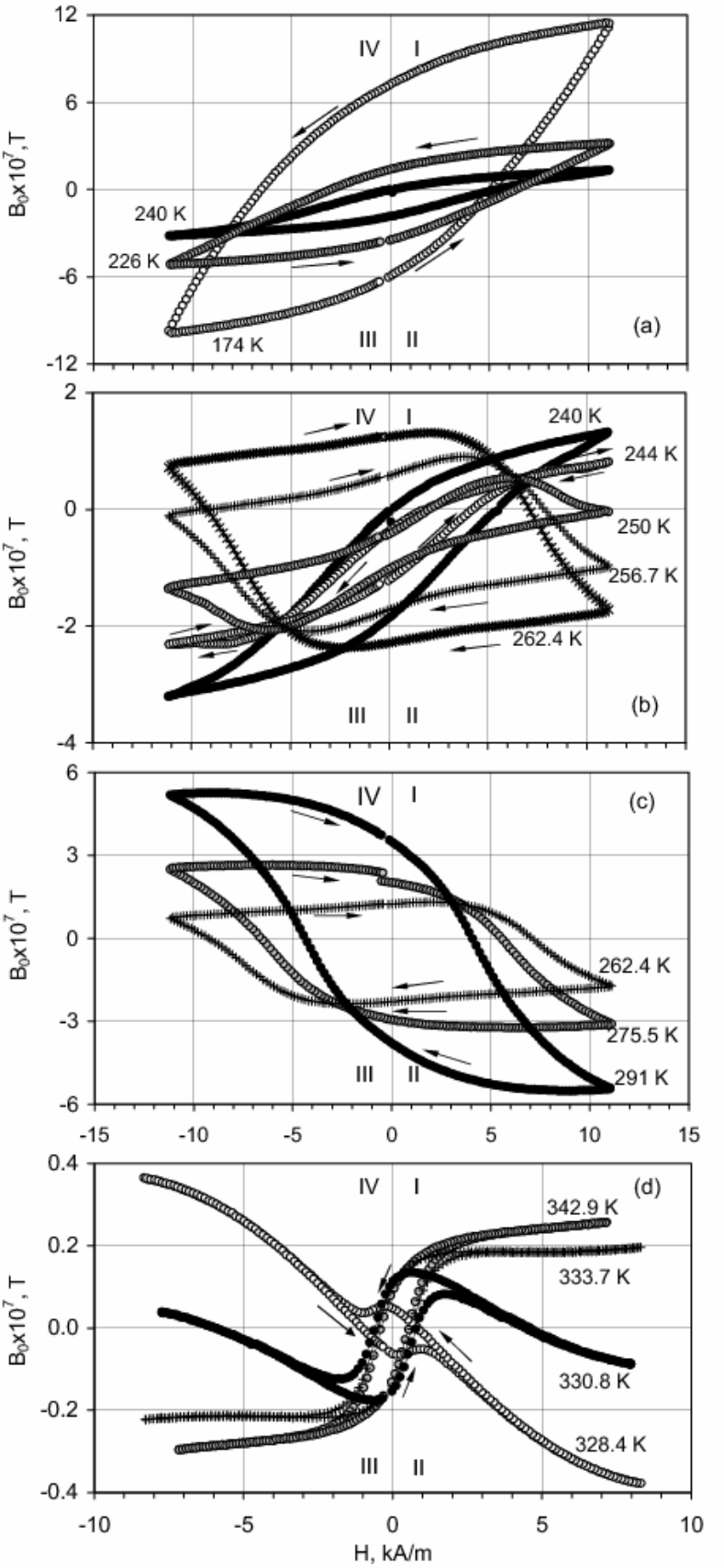

Figure 8. Real part of the stress-induced induction versus cyclic polarizing field for a slowly cooled sample

#2 of a Ni-Fe-Ga-Co alloy for temperature ranges 170-240 K (a), 240-260 K (b), 260-290 K (c) and 329-343 K (d). Oscillatory strain amplitude 2×10^{-5}, frequency of the cyclic polarizing field 0.002 Hz. Arrows show directions of circulation along the loops.

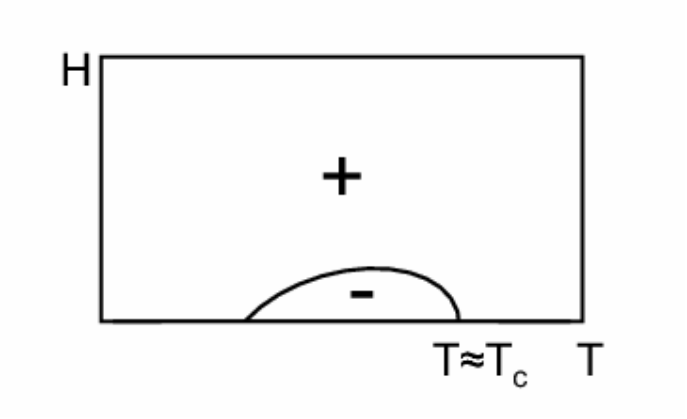

Figure 9. Schematic representation of the position of Villari critical line separating regions of positive and negative magnetostriction on *H-T* plane.

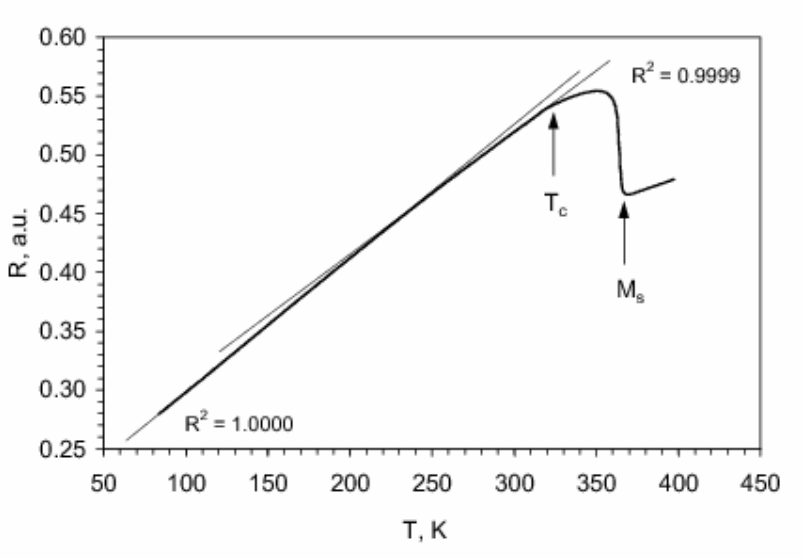

Figure 10. Temperature dependence of the resistance (in arbitrary units) of a slowly cooled sample of a Ni-Fe-Ga-Co alloy. Thin lines show fittings of the two parts of the dependence (below 240 K and between 240 K and the Curie temperature, T_c, by linear functions.

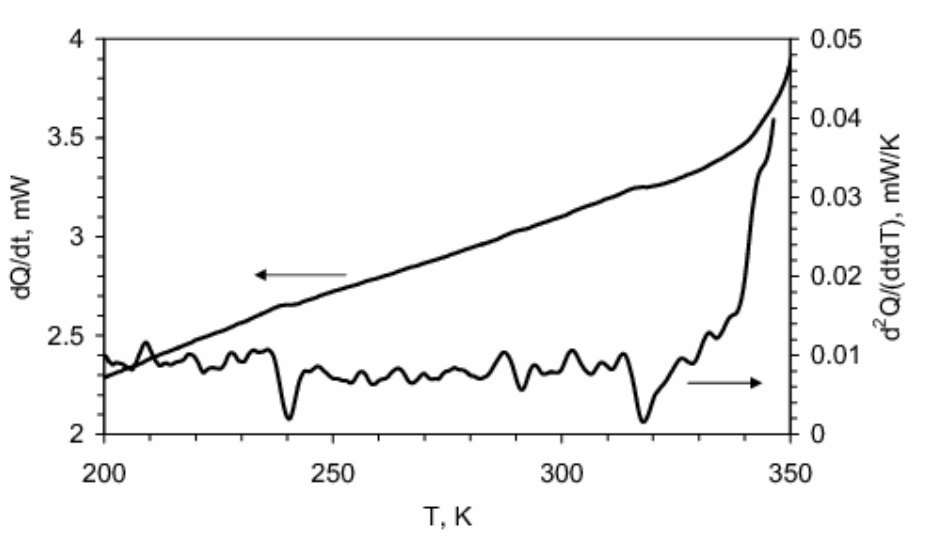

Figure 11. Heat flow *dQ/dt* and its temperature derivative $d^2Q/dtdT$ registered during cooling scan for a slowly cooled sample of a Ni-Fe-Ga-Co alloy. The increase of the heat flow and its derivative on the high-temperature side of the plot corresponds to the martensitic transformation range.